FLORE
Repository istituzionale dell'Università degli Studi di Firenze

Heat and mass transfer coefficients of falling-film absorption on a partially wetted horizontal tube

(Article begins on next page)

11 July 2022

Heat and mass transfer coefficients of falling-film absorption on a partially wetted horizontal tube

Niccolò Giannetti[1*], Andrea Rocchetti[2], Seiichi Yamaguchi[1], Kiyoshi Saito[1]

[1] Department of Applied Mechanics and Aerospace Engineering, Waseda University
3-4-1 Okubo, Shinjuku-ku, Tokyo 169-8555, Japan
[2] Department of Industrial Engineering of Florence, University of Florence
Via Santa Marta 3, Firenze, 50139, Italy
[*] Corresponding author: niccolo@aoni.waseda.jp

Abstract- Detailed, reliable, and time-saving methods to predict the transfer characteristics of horizontal-tube falling-film absorbers are critical to control system operability, such that it is closer to its technical limitations, and to optimise increasingly complex configurations. In this context, analytical approaches continue to hold their fundamental importance. This study presents an analytical solution of the governing transport equations of film absorption around a partially wetted tube. A film stability criterion and a wettability model extend the validity range of the resulting solution and increase its accuracy. Temperature and mass fraction fields are analytically expressed as functions of Prandtl, Schmidt, and Reynolds numbers as well as tube dimensionless diameter and wetting ratio of the exchange surface. Inlet conditions are arbitrary. The Lewis number and a dimensionless heat of absorption affect the characteristic equation and the corresponding eigenvalues. Consequently, local and average transfer coefficients are estimated and discussed with reference to the main geometrical and operative parameters. Finally, a first comparison with the numerical solution of the problem and experimental data from previous literature is presented to support the simplifying assumptions, which are introduced and as a first model validation.

34 **Nomenclature**

35 A, B — Eigenfunction coefficients

36 a, b — Power series coefficients

37 c_p — Isobaric specific heat, $J \cdot kg^{-1}K^{-1}$

38 D — Mass diffusivity, $m^2 \cdot s^{-1}$

39 d — Diameter, m

40 E, H — Single variable exponential functions

41 F, G — Eigenfunctions

42 g — Gravity, $m \cdot s^{-2}$

43 h — Specific enthalpy, $kJ \cdot kg^{-1}$

44 htc — Heat transfer coefficient, $kW \cdot m^{-2}K^{-1}$

45 k — Thermal conductivity, $W \cdot m^{-1}K^{-1}$

46 l — Reference axial length, m

47 L_c — Characteristic length, m $[L_c = \nu^{2/3} \cdot g^{-1/3}]$

48 Le — Lewis number $[Le = \alpha \cdot D^{-1}]$

49 mtc — Mass transfer coefficient, $m \cdot s^{-1}$

50 Nu — Nusselt number $[Nu = htc\, L_c \cdot k^{-1}]$

51 P — Pressure, kPa

52 Pr — Prandtl number $[Pr = \nu \cdot \alpha^{-1}]$

53 Q — Heat flux, W

54 r — Outer tube radius, m

55 Re — Reynolds Number $[Re = 4\Gamma \cdot \mu^{-1}]$

56 S — Area, m^2

57 Sc — Schmidt Number $[Sc = \mu \cdot \rho^{-1}D^{-1}]$

58 Sh — Sherwood Number $[Sh = mtc\, L_c \cdot D^{-1}]$

59 t — Tube wall thickness, m

60 T — Temperature, K

61 u — Streamwise Velocity, $m \cdot s^{-1}$

62 v — Normal Velocity, $m \cdot s^{-1}$

63 W — Transversal extension of the wet part, m

64 WR — Wetting Ratio

65 x — Local tangential position, m

66 y — Local normal position, m

67

68 **Greek symbols**

69 α — Thermal diffusivity, $m^2 \cdot s^{-1}$

70 β — Contact angle

71 ε — Dimensionless tangential position

72 γ — Dimensionless LiBr mass fraction

73 distribution

74 η — Dimensionless normal position

75 Λ — Normalised heat of absorption

76 $[\Lambda = h_{abs}(\omega_e - \omega_{in}) \cdot (T_e - T_{in})^{-1} \omega_e^{-1} c_p^{-1}]$

77 λ, ϕ — Eigenvalues

78 θ — Dimensionless temperature distribution

79 Γ — Mass flow rate per unit length, $kg \cdot s^{-1}m^{-1}$

80 δ — Film thickness, m

81 μ — Dynamic viscosity, $Pa \cdot s$

82 ρ — Density, $kg \cdot m^{-3}$

83 ω — LiBr mass fraction

84

85 **Subscripts**

86 0 — Film breaking condition

87 abs — Absorption

88 av — Average

89 b — Bulk value

90 c — Cooling water side

91 e — Equilibrium

92 g — Global

93 i — Power series index

94 if — Interface

95 in — Inlet

96 max — Maximum

97 n, m — Eigenvalue/Eigenfunction indexes

98 o — Outlet

99 sat — Phases equilibrium

100 T — Temperature

101 v — Vapour

102 W — Wall

103   105   *   Dimensionless

104 **Superscripts**

106

1. Introduction

108 It is not possible to consider heat transfer and mass transfer
109 separately in several technical circumstances and physical
110 processes. Absorption systems, such as chillers, heat amplifiers,
111 and heat transformers, belong to the aforementioned category and
112 represent an opportunity for clean and efficient energy
113 conversion systems (1). The main advantages of these systems
114 include low-grade heat as the main energy source, higher
115 reliability, and environmentally friendly refrigerants. This is
116 accompanied by the possibility of realising the refrigerant
117 pressure jump in a liquid phase. Accordingly, the compressor of
118 a conventional system is substituted with a set of components,
119 such as a solution pump, a generator, an absorber, and a
120 solution heat exchanger, termed as a "thermal compressor". As a
121 downside, this requires a significantly larger exchange surface.
122 In addition, extant studies indicated that the highest amount of
123 irreversibility occurs in an absorber (2) and that global
124 capacity and first law efficiency are limited by the amount of
125 refrigerant that is absorbed in this component (3-4). Therefore,
126 the intensification of the absorption process and proper design
127 of an absorber are the critical factors that should be addressed.
128 Conversely, the recent technical development of absorption
129 chillers, heat pumps, and heat transformers corresponds to
130 increasingly complex plant configurations (5-6), and
131 specifically constitutes a step forward with respect to the
132 theoretical background required for an accurate performance
133 prediction, optimisation, and control. In general, the systems
134 design approach continues to rely on empirical rules, heuristic
135 correlations, or trial and error procedures on a global and
136 component scale. The correlations rely on large sets of data, in
137 which each set depends on experimental equipment as well as the

138 specific boundary conditions of these measurements. Furthermore,
139 devices that are designed to achieve high performance under
140 nominal conditions may not exhibit a sufficient performance over
141 most of the actual operative range. Similarly, in practice,
142 conditions are transient and change continuously, because they
143 are affected by interrelations with the external environment.
144 Consequently, instantaneous conditions significantly differ from
145 the design point. The construction of reliable and widely
146 applicable theoretical models enables the design, optimisation,
147 and definition of an effective control method without depending
148 on trial and error procedures or empirical rules.
149 More specifically, horizontal-tube falling-film absorbers can
150 realise high heat and mass transfer rates with compact size and
151 negligible pressure losses. Nevertheless, prior experimental
152 studies on falling film absorption (7-12) report a limited
153 amount of results with high uncertainties and within a
154 relatively narrow range of operative conditions.
155 Reference (13) numerically discusses a model for film absorption
156 and desorption of a laminar liquid film with constant thickness
157 that flows over a vertical isothermal plate. A similar model was
158 applied by (14) to a horizontal tube heat exchanger. References
159 (15-18) introduce the effects of thickness and velocity
160 distributions around a tube surface via numerical analyses.
161 Finally, references (19-25) use the Volume of Fluid technique to
162 examine and extract detailed descriptions of the wavy film
163 dynamics, inter-tube droplets formation, detachment, and impact.
164 Numerical analysis and computational fluid dynamics (CFD) are
165 powerful tools that could be very precise when the problem is
166 properly formulated. However, it is necessary to adequately
167 consider the time required to reach an accurate solution and the
168 fact that its validity is restricted to the specific case and
169 the selected operative condition. Generalisable design
170 guidelines are not directly provided by specific results as well
171 as heuristic methods. Given this viewpoint, analytical
172 approaches continue to maintain their fundamental importance to

173 capture the physics of the problem and generalise the validity
174 of the solution. The main limitations of extant analytical
175 models include the geometry of the solid surface, assumptions of
176 complete wetting, equilibrium of an inlet solution with the
177 refrigerant vapour, uniform velocity profile, and film thickness
178 (26–29). Reference (28) indicated that uniform velocity profile
179 and film thickness are responsible for approximately 20%
180 deviations in the heat and mass transfer coefficients, and they
181 under-predict approximately 40% of the distance required for the
182 development of the thermal boundary layer. Therefore, this study
183 successfully achieves an accurate and widely applicable
184 analytical solution of the governing equations of falling film
185 absorption over a horizontal tube including the effects of
186 thickness variations, incomplete wetting, and the corresponding
187 reduction in transfer interfaces.
188
189 **2. Physical model**

190 The present analysis focuses on an absorptive liquid film flowing
191 over a vertical row of horizontal smooth tubes. Droplet impact
192 and hydrodynamic boundary layer development (19–25, 30) are not
193 discussed herein. Figure 1 schematically illustrates the system
194 under consideration. A single tube at uniform wall-temperature,
195 T_w, is considered. A thin film of LiBr-H_2O solution impinges at
196 the top (x=0) and flows viscously down the tube due to gravity as
197 a laminar incompressible liquid. Additionally, absorption can
198 occur at the free-interface of the film based on the thermo-
199 physical relation between the solution and the vapour. The
200 enthalpy of vapour condensation that is released in the lithium-
201 bromide/water mixture is rejected to the cooling water flowing
202 inside the tube. Following the development of the thermal
203 boundary layer, the temperature gradient related to the cooling
204 process at the wall also influences the temperature at the
205 interface, and this in turn establishes the equilibrium mass

206 fraction at the vapour pressure within the heat exchanger and
207 consequently controls mass transfer.
208
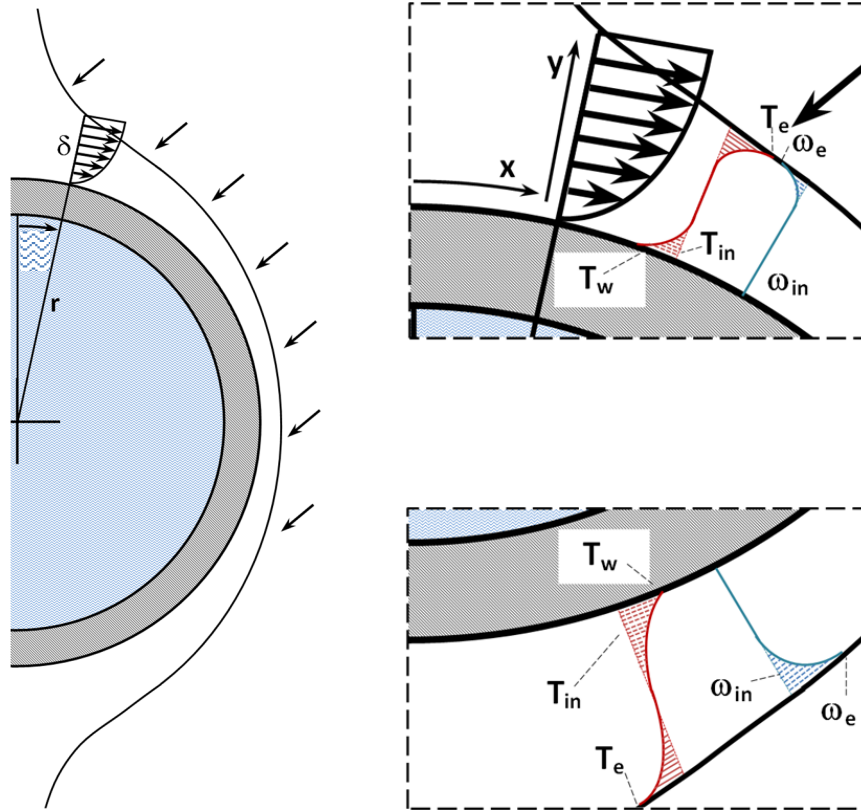
Figure 1. Local coordinate system

212 In order to reach a closed analytical solution of the governing
213 transport equations, heat and mass transfer processes are
214 considered under the following main assumptions:
215 – The zone of impingement is assumed as a small fraction of the
216 total periphery, and it is assumed that the thermal boundary
217 layer starts its growth from the upper stagnation point ($x \approx 0$);
218 – It is assumed that both the tube circumference and length are
219 large when compared to the film thickness and that the
220 disturbances at the edges of the system can be neglected;
221 – The flow is laminar;
222 – Neither interfacial shear forces with the vapour nor
223 interfacial waves exist;

224 – Thermodynamic equilibrium occurs at the film inlet–interface
225 with the vapour at the heat exchanger pressure, and thus mass
226 transfer occurs without any resistance;
227 – Thermo-physical solution properties are similar to those of an
228 ideal mixture and remain constant along the film thickness and
229 around the tube. As a corollary, natural and Marangoni convection
230 are not considered;
231 – Heat transfer to the vapour environment is neglected;
232 – The variation of the mass flowrate due to the absorbed vapour
233 is negligible;
234 – According to the thin film approximation introduced by (27),
235 body fitted coordinates (*x* along the tube surface and *y* normal to
236 it at any point) are used because the film thickness is low when
237 compared to the tube diameter.
238 A curvilinear coordinate transformation is adopted to map the
239 flow domain of the physical space to a simple rectangular domain
240 (16). The dimensionless variables considered in the
241 circumferential and radial directions correspond to $\varepsilon=x/\pi r$ and $\eta=y/\delta$,
242 respectively. Tangential (eq. 1) and normal (eq. 2) velocity
243 components based on the Nusselt integral solution of the boundary
244 layer momentum and continuity equations with constant properties
245 form (see, for instance, references 13–18) are employed under the
246 assumption that the momentum transfer of the fluid is dominated
247 by viscous forces in the absence of inertia and pressure forces.
248

249
$$u = \frac{\rho g \delta^2}{2\mu} \sin \pi\varepsilon \left(2\eta - \eta^2\right) \tag{1}$$

250
$$v = -\frac{\rho g \delta^2 \eta^2}{2\mu r} \left[\frac{1}{\pi}\frac{d\delta}{dx}\sin \pi\varepsilon + \delta\left(1 - \frac{\eta}{3}\right)\cos \pi\varepsilon\right] \tag{2}$$

251

252 Accordingly, once the film mass flowrate per unit length of the
253 tube is known, the corresponding film thickness is given by eq.
254 3.

255 $$\delta = \left(\frac{3\mu\Gamma}{\rho^2 g \sin \pi\varepsilon} \right)^{1/3}$$ (3)

256 A small thermal resistance is associated with a thinner film at
257 low specific mass flowrates, and thus moving the operability of
258 falling film absorbers to a low Reynolds number is attractive in
259 increasing the performance of absorption systems and reducing
260 their overall size. However, it is necessary to consider the
261 reduction in the contact area due to partial wetting as a
262 critical related issue. In these operative conditions,
263 specifically at a low film Reynolds number ($Re=4\Gamma/\mu$) and while
264 employing liquids with high surface tension (i.e., low Weber
265 numbers), it is not possible to consider the assumptions of a
266 film with uniform thickness and complete wetting of the transfer
267 surface as even approximately rigorous. This leads to an
268 unacceptable inaccuracy of simulation results (i.e., the
269 obtained trend of the predicted heat transfer coefficient itself
270 disagrees with measurements (31)). Furthermore, it is recognised
271 that partial wetting occurs even at typical operative conditions.
272 Among the previously proposed models, the effect of the amount
273 of wetted surface is not assessed or is merely assumed as a
274 fixed value imposed on the calculation (15, 32) albeit with a
275 few exceptions (9, 33–35). Moreover, related experimental data
276 and visual descriptions by digital image processing are also
277 extremely limited in terms of the number of studies that report
278 the same as well as in the range of conditions that is covered
279 (36–39). Nevertheless, the role of wettability is recognised as
280 a dominant factor in determining the efficiency of the
281 absorption process. Therefore, both a criterion of stability of
282 the uniform film to identify the minimum flow rate to ensure a
283 complete wetting of the surface and a method to estimate the
284 wetted area after the film breakage should be included to
285 enhance the model capability to predict the performance of these
286 devices.

287 To consider the effect of partial wetting, after the thermo-
288 physical properties of the solution are given, the extension of
289 the range affected by the phenomenon is identified by the
290 critical condition for a uniform film in terms of minimum wetting
291 rate Γ_0 that corresponds to a critical Reynolds number Re_0. The
292 latter can be experimentally measured (37–41) or analytically
293 estimated for a surface with generic inclination (42–43) once the
294 characteristic contact angle that is representative of the
295 affinity of the solid–liquid interaction is known. Among the
296 various available methods (44–47), the principle of minimising
297 the energy contained in a given stream wise length of the
298 falling film is hereby used to assess the stability of the
299 uniform configuration (eq. 4) and to provide an estimate (eq. 5)
300 of the rivulet wetting ability (42–43) given the assumption of a
301 rivulet cross-section geometry. The value of the dimensionless
302 group $(Re_0 \cdot We_0^3)^{1/15}$ in (43) is directly proportional to the
303 dimensionless critical thickness δ_0^* that is defined in (42) (eq.
304 4). Therefore, equation 4 represents the flow regime transition
305 between a uniform film and a rivulet flow configuration with
306 circular cross-section shape and contact angle β, which
307 partially wets the solid surface. This is obtained from the
308 condition of equivalent kinetic plus surface tension energy, and
309 flowrate of the two regimes, when the stable condition of the
310 rivulet is identified through the principle of minimum energy.
311

$$312 \quad \delta_0^{*5} + (1 - \cos\beta) - G(\beta)\delta_0^{*3} = 0 \qquad , \qquad \delta_0^* = \left(\frac{\rho^3 g^2}{15\mu^2\sigma}\right)^{1/5}\delta_0 \qquad\qquad (4)$$

313 Equation 5 corresponds to the minimisation of the energy
314 contents of a given stream-wise length of the rivulet, with
315 respect to the geometrical parameter that defines its wetting
316 ability WR (the ratio of the base of the rivulet w to the total
317 axial length l taken as a reference).
318

319 $$WR = \left\{ \frac{1}{15} \frac{\rho g}{\sigma} \frac{\psi(\beta)}{\sin\beta} \left[\frac{\beta}{\sin\beta} - \cos\beta \right]^{-1} \right\}^{3/5} \frac{\sin\beta}{\gamma(\beta)} \mathrm{Re} \qquad (5)$$

320

321 where $G(\beta)$, $\psi(\beta)$, and $\gamma(\beta)$ denote geometrical functions of the contact

322 angle β between the liquid-gas interface of the rivulet (further

323 details are given in reference 43). When WR is used to estimate

324 the wetting ability of the film along the absorber tube, its

325 value corresponds to the ratio of the wetted portion w to the

326 tube unit length l (Figure 2).

327 For lower solution flowrates, methods based on the principle of

328 minimum energy (eq. 5) as well as experiments (37-41, 43) are in

329 agreement with a linearised wettability model (eq. 6) relative to

330 the film Reynolds number, which gives zero wetting when Reynolds

331 number is zero, and complete wetting at $Re=Re_0$.

332

333 $$WR = \frac{\mathrm{Re}}{\mathrm{Re}_0} \qquad (6)$$

334

335 Therefore, δ_0^* can be evaluated from eq. 4, once the value of the

336 characteristic contact angle of the liquid-solid pair is known.

337 Afterwards, using the Nusselt velocity profile for a vertical

338 falling film, the film thickness can be directly related to the

339 film Reynolds number ($Re=4\Gamma/\mu$) and the critical Reynolds number

340 at which the film breaking occurs Re_0 is calculated as in eq. 7.

341 $$\mathrm{Re}_0 = \left(\frac{3^5 g \mu^4}{4^5 15^3 \rho \sigma^3} \right)^{-1/5} \delta_0^{*3} \qquad (7)$$

342 The approach aims at estimating the wetted exchange area on an

343 average basis while not targeting a local description of the

344 complex film hydrodynamics. Furthermore, a closed solution

345 requires considering WR as an independent function of the angular

346 position on the tube surface. Accordingly, the film thickness

347 distribution (eq. 9) is adjusted to assure the consistency

348   between uniform and partial wetting configurations (eq. 8) by

349   using a modified form of the Nusselt equation (as in (32)).
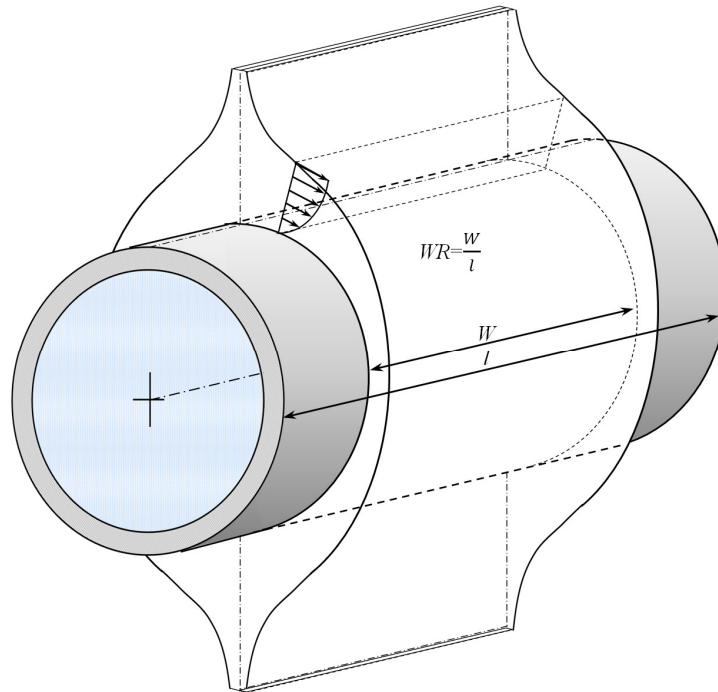
350

351

$$352 \quad \frac{\Gamma}{2WR} = \int_0^\delta \rho u(y) dy = \frac{1}{3} \frac{\rho^2 g \sin \beta}{\mu} \delta^3 \qquad (8)$$

$$353 \quad \delta = \left(\frac{3\mu\Gamma}{WR\rho^2 g \sin \pi\varepsilon} \right)^{1/3} \qquad (9)$$

354

355   To the authors' knowledge, a direct validation of eq. 9 has not

356   been achieved in previous literature and further research efforts

357   in this regard are needed.

358

360   **Figure 2. A physical model of film partial wetting**

361

362   Heat and mass transfer characteristics of the system under

363   analysis are studied with reference to eq.s 10 and 11. This two-

364   dimensional form of the energy and species transport equations is

365   written for a steady flow with constant properties without

366   internal heat generation and viscous dissipation and neglecting

367 diffusion terms in the flowing direction (see, for instance, 15–
368 16, 27).
369

370
$$\frac{\partial T}{\partial \varepsilon} = \frac{\pi r \alpha}{u \delta^2} \frac{\partial^2 T}{\partial \eta^2} + \left(\frac{\eta}{\delta} \frac{d\delta}{d\varepsilon} - \frac{\pi r v}{u \delta} \right) \frac{\partial T}{\partial \eta}$$
(10)

371
$$\frac{\partial \omega}{\partial \varepsilon} = \frac{\pi r D}{u \delta^2} \frac{\partial^2 \omega}{\partial \eta^2} + \left(\frac{\eta}{\delta} \frac{d\delta}{d\varepsilon} - \frac{\pi r v}{u \delta} \right) \frac{\partial \omega}{\partial \eta}$$
(11)

372
373 Where,
374

375
$$\frac{d\delta}{d\varepsilon} = -\left(\frac{\mu \Gamma \pi^3}{9 W R \rho^2 g} \right)^{1/3} \frac{1}{\sin^{1/3} \pi \varepsilon} \frac{1}{\tan \pi \varepsilon}$$
(12)

376
377 It is shown that eq. 13 is generally applicable for the velocity
378 distribution expressed in eq. 1 and eq. 2.
379

380
$$\left(\frac{\eta}{\delta} \frac{d\delta}{d\varepsilon} - \frac{\pi r v}{u \delta} \right) = 0$$
(13)

381
382 As a result, the simplified expression is obtained as follows:
383

384
$$\frac{\partial T}{\partial \varepsilon} = \frac{\pi r \alpha}{u \delta^2} \frac{\partial^2 T}{\partial \eta^2}$$
(14)

385
$$\frac{\partial \omega}{\partial \varepsilon} = \frac{\pi r D}{u \delta^2} \frac{\partial^2 \omega}{\partial \eta^2}$$
(15)

386
387 An analytical solution of the coupled set of equations is
388 approached with the final aim of obtaining Nusselt and Sherwood
389 number expressions in terms of the operative parameters,
390 geometrical features, and boundary conditions.
391 It is advantageous for the solution of the problem to use a
392 dimensionless form of the variables T and ω as defined by eqs. 16–
393 17 where T_e and ω_e are defined in (28). These values are,

394 respectively, the equilibrium temperature of the solution at **LiBr**

395 mass fraction ω_n and the equilibrium LiBr mass fraction of the

396 solution at temperature T_{in}, namely, the temperature and the mass

397 fraction reached if thermodynamic equilibrium is obtained without

398 changes in mass fraction and temperature.

399

400 $$\theta(\varepsilon,\eta) = \frac{T(\varepsilon,\eta) - T_W}{T_e - T_W} \tag{16}$$

401 $$\gamma(\varepsilon,\eta) = \frac{\omega(\varepsilon,\eta) - \omega_{in}}{\omega_e - \omega_{in}} \tag{17}$$

402

403 Accordingly, $T_e - T_W$ represents the level of sub-cooling of the wall

404 while $\omega_e - \omega_n$ embodies the driving force for vapour diffusion at the

405 inlet of the calculation domain. The dimensionless tube diameter

406 $d^* = 2\pi r / L_C$ is defined as the ratio of the tube circumference to the

407 characteristic length L_C, which is expressed in eq. 18 as follows

408 (17):

409

410 $$L_C = \left(\frac{\mu^2}{\rho^2 g}\right)^{1/3} \tag{18}$$

411

412 Finally, non-constant terms of eq.s 14 and 15 are developed and

413 dimensionless variables and parameters are used to express energy

414 and species transport equations in eq. 19 and eq. 20,

415 respectively, in which the independent variables are separated

416 between the sides of the equations as follows:

417

418 $$\frac{1}{d^* \sin^{1/3} \pi\varepsilon} \left(\frac{3\,\mathrm{Re}}{4WR}\right)^{4/3} \frac{\partial \theta}{\partial \varepsilon} = \frac{1}{\mathrm{Pr}\left(2\eta - \eta^2\right)} \frac{\partial^2 \theta}{\partial \eta^2} \tag{19}$$

419 $$\frac{1}{d^* \sin^{1/3} \pi\varepsilon} \left(\frac{3\,\mathrm{Re}}{4WR}\right)^{4/3} \frac{\partial \gamma}{\partial \varepsilon} = \frac{1}{Sc\left(2\eta - \eta^2\right)} \frac{\partial^2 \gamma}{\partial \eta^2} \tag{20}$$

420

421 The solution is approached with the following boundary and inlet
422 conditions: solution temperature and mass fraction at the
423 distributor or, by assuming that complete mixing occurs, the bulk
424 values of the solution coming from the previous tube ($x\approx0$ and
425 $0<y<\delta$; $T=T_{in}$, $\theta(0,\eta)=\theta_{in}$; $\omega=\omega_{in}$, $\gamma(0,\eta)=0$), at the tube wall constant
426 temperature and non-permeability to species are assured ($y=0$;
427 $T=T_w$, $\theta(\varepsilon,0)=0$; $\partial\omega/\partial y=0$, $\partial\gamma/\partial\eta\big|_{w}=0$), and at the phase interface
428 ($y=\delta$, $T=T_{sat}(\omega_{if},P)$, $\omega=\omega_{if}$) phase equilibrium is established.
429

430
$$\left.\frac{\partial\theta}{\partial\eta}\right|_{if} = \frac{\Lambda}{Le}\left.\frac{\partial\gamma}{\partial\eta}\right|_{if} \tag{21}$$

431

432 Equation 21 constitutes a rearrangement of Fick's law of
433 diffusion and Fourier law that assures that the heat produced by
434 absorption at the film interface is conducted through the film
435 towards the tube surface. Where, the following expression holds
436 and defines the normalised heat of absorption (28):

437

438
$$\Lambda = -\frac{h_{abs}\left(\omega_e - \omega_W\right)}{\omega_e c_p\left(T_e - T_W\right)} \tag{22}$$

439

440 Additionally, with respect to the vapour pressure equilibrium at
441 the interface, a linear relation (as in (28)) between temperature
442 and mass fraction at the film interface is employed. Accordingly,
443 in terms of the dimensionless variables at a constant pressure,
444 the relation expressed by eq. 23 is obtained.

445

446
$$\gamma_{if} = 1 - \theta_{if} \tag{23}$$

447 Equation 23 was found in good agreement for a wide range of
448 operative conditions of LiBr-H$_2$O solution and a thermodynamic
449 justification (although it limited to electrolytic solutions) was
450 presented in reference (48).

451

452 **3. Solution method**

453   The dependent functions (eq.s 24-25) are assumed as a infinite
454   series of products of a number of eigenfunctions in which each is
455   dependent on a single variable as shown in (12) and (13).
456

457    $$\theta(\varepsilon,\eta) = \sum_{n=1}^{\infty} A_n F_n(\eta) E_n(\varepsilon) \tag{24}$$

458    $$\gamma(\varepsilon,\eta) = 1 - \sum_{n=1}^{\infty} B_n G_n(\eta) H_n(\varepsilon) \tag{25}$$

459

460   The application of this method results in four ordinary
461   differential equations as follows:
462

463    $$\frac{1}{d^* \sin^{1/3} \pi\varepsilon} \left(\frac{3\,\mathrm{Re}}{4WR}\right)^{4/3} \frac{E_n{'}}{E_n} = \frac{1}{\mathrm{Pr}\left(2\eta - \eta^2\right)} \frac{F_n{''}}{F_n} = -\lambda_n^2 \tag{25}$$

464    $$\frac{1}{d^* \sin^{1/3} \pi\varepsilon} \left(\frac{3\,\mathrm{Re}}{4WR}\right)^{4/3} \frac{H_n{'}}{H_n} = \frac{1}{Sc\left(2\eta - \eta^2\right)} \frac{G_n{''}}{G_n} = -\phi_n^2 \tag{27}$$

465

466   The general solutions of the left members of both eq. 26 and eq.
467   27 are as follows:
468

469    $$E_n(\varepsilon) = e^{-\lambda_n^2 d^* \left(\frac{4WR}{3\,\mathrm{Re}}\right)^{4/3} \int_0^\varepsilon \sin^{1/3} \pi\varepsilon\, d\varepsilon} \tag{28}$$

470    $$H_n(\varepsilon) = e^{-\phi_n^2 d^* \left(\frac{4WR}{3\,\mathrm{Re}}\right)^{4/3} \int_0^\varepsilon \sin^{1/3} \pi\varepsilon\, d\varepsilon} \tag{29}$$

471

472   Where λ_n and ϕ_n denote the eigenvalues corresponding to the
473   eigenfunctions F_n and G_n, respectively. Additionally, for the
474   linear equilibrium condition at the interface (eq. 23) that
475   should be satisfied for every ε, it is necessary for every n that
476    $\lambda_n = \phi_n$. The boundary conditions at the wall require $F_n(0)=0$ and
477    $G_n{'}(0)=0$, while eq. 30 and eq. 31 are obtained at the interface.
478

479 $$A_n F_n(1) = B_n G_n(1) \tag{30}$$

480 $$A_n F_n{}'(1) = -\frac{\Lambda}{Le} B_n G_n{}'(1) \tag{31}$$

481

482 Equation 30 and eq. 31 represent two homogeneous equations for A_n

483 and B_n, and thus a non-null solution is reached given the

484 condition that the determinant equals zero.

485

486 $$\frac{F_n{}'(1)}{F_n(1)} = -\frac{\Lambda}{Le}\frac{G_n{}'(1)}{G_n(1)} \tag{32}$$

487

488 Equation 32 represents the characteristic equation to determine

489 the eigenvalues λ_n when the solution for F_n and G_n is determined.

490 The power series solutions for the right-side members of eq. 26

491 and eq. 27 are expressed as follows:

492

493 $$F_n(\eta) = \sum_{i=0}^{\infty} a_{n,i}\eta^i \tag{33}$$

494 $$G_n(\eta) = \sum_{i=0}^{\infty} b_{n,i}\eta^i \tag{34}$$

495

496 The boundary conditions at the wall $F_n(0)=0$ and $G_n'(0)=0$, namely

497 constant temperature and non-permeability to species , are used

498 to calculate the coefficients $a_{n,i}$ and $b_{n,i}$ by the recursive

499 relations represented by eq. 35 and eq. 36, respectively.

500

501 $$a_{n,0} = 0, a_{n,1} = 1, a_{n,2} = 0, a_{n,3} = 0, a_{n,i} = \frac{\lambda_n^2 \Pr\left(a_{n,i-4} - 2a_{n,i-3}\right)}{i(i-1)}, i \geq 4 \tag{35}$$

502 $$b_{n,0} = 1, b_{n,1} = 0, b_{n,2} = 0, b_{n,3} = -\lambda_n^2\Big/3 ,$$

503 $$b_{n,i} = \frac{\lambda_n^2 Sc\left(b_{n,i-4} - 2b_{n,i-3}\right)}{i(i-1)}, i \geq 4 \tag{36}$$

504

505 The coefficients A_n and B_n are determined by using a Sturm–
506 Liouville orthogonality condition at the inlet and the boundary
507 conditions at the interface. The solution method follows the
508 procedure presented in (28) although the inlet temperature value
509 in this case is different from the constant value at the wall.
510 Equations 37 and 38 are expressed by multiplying the right-side
511 members of eq. 26 and eq. 27 by the eigenfunctions F_m and G_m,
512 respectively, in the specified order and integrating with respect
513 to η. This is expressed as follows:

514

515
$$\lambda_n^2 \Pr \int_0^1 \left(2\eta - \eta^2\right) F_m F_n d\eta = -\int_0^1 F_m F_n \, '' d\eta = F_m(0) F_n\,'(0) - F_m(1) F_n\,'(1) + \int_0^1 F_m\,' F_n\,' d\eta \qquad (37)$$

516
$$\lambda_n^2 Sc \int_0^1 \left(2\eta - \eta^2\right) G_m G_n d\eta = -\int_0^1 G_m G_n \, '' d\eta = G_m(0) G_n\,'(0) - G_m(1) G_n\,'(1) + \int_0^1 G_m\,' G_n\,' d\eta \qquad (38)$$

517

518 The corresponding equations (obtained by proceeding in the same
519 way for eigenvalues and eigenfunctions with index m) are
520 subtracted and the boundary conditions expressed in eq. 30 and eq.
521 31 are used to yield eq. 39 and eq. 40 as follows:

522

523
$$\Pr\left(\lambda_n^2 - \lambda_m^2\right)\int_0^1 \left(2\eta - \eta^2\right) F_n F_m d\eta = F_n(1) F_m\,'(1) - F_m(1) F_n\,'(1) \qquad (39)$$

524
$$Sc\left(\lambda_n^2 - \lambda_m^2\right)\int_0^1 \left(2\eta - \eta^2\right) G_n G_m d\eta = G_n(1) G_m\,'(1) - G_m(1) G_n\,'(1) \qquad (40)$$

525

526 The coupling between the previous two conditions is established
527 by using eq. 30 and eq. 31 as follows:

528

529
$$F_n(1) F_m\,'(1) - F_m(1) F_n\,'(1) = -\frac{\Lambda}{Le}\frac{B_n B_m}{A_n A_m}\left[G_n(1) G_m\,'(1) - G_m(1) G_n\,'(1)\right] \qquad (41)$$

530

531 Equation 41 enables the combination of eq. 39 and eq. 40 as
532 follows:

533

$$Sc\left(\lambda_n^{\,2}-\lambda_m^{\,2}\right)\int_0^1\left(2\eta-\eta^2\right)\left(\Pr LeA_nA_mF_nF_m+Sc\Lambda B_nB_mG_nG_m\right)d\eta=0 \tag{42}$$

535

536 This directly implies,

537

$$\int_0^1\left(2\eta-\eta^2\right)\left(\Pr LeA_nA_mF_nF_m+Sc\Lambda B_nB_mG_nG_m\right)d\eta\begin{cases}=0,n\neq m\\ \neq 0,n=m\end{cases} \tag{43}$$

539

540 The boundary conditions of constant temperature and mass fraction
541 are used over the entire film thickness at the inlet of the
542 calculation domain as follows:

543

$$\sum_{n=1}^{\infty}A_nF_n(\eta)=\theta_{in} \tag{44}$$

$$\sum_{n=1}^{\infty}B_nG_n(\eta)=1 \tag{45}$$

546

547 The summation of the integrals is simplified as follows:

548

$$\sum_{n=1}^{\infty}\int_0^1\left(2\eta-\eta^2\right)(\Pr LeA_nA_mF_nF_m+Sc\Lambda B_nB_mG_nG_m)d\eta=\int_0^1\left(2\eta-\eta^2\right)(\Pr Le\theta_{in}A_mF_m+Sc\Lambda B_mG_m)d\eta$$

550 $$\tag{46}$$

551 According to eq. 43, the first relation between A_n and B_n can be
552 obtained in eq. 44, while the second relation is expressed by
553 either eq. 30 or eq. 31.

554

$$\int_0^1\left(2\eta-\eta^2\right)(\Pr LeA_n^{\,2}F_n^{\,2}+Sc\Lambda B_n^{\,2}G_n^{\,2})d\eta=\int_0^1\left(2\eta-\eta^2\right)(\Pr Le\theta_{in}A_nF_n+Sc\Lambda B_nG_n)d\eta \tag{47}$$

556

557 Finally, A_n and B_n are solved for as follows:

558

$$559 \quad A_n = B_n \frac{G_n(1)}{F_n(1)} \tag{48}$$

$$560 \quad B_n = \frac{\int\limits_0^1 \left(2\eta - \eta^2\right)\left(\Pr Le\,\theta_{in}\,\dfrac{G_n(1)}{F_n(1)}F_n(\eta) + Sc\Lambda G_n(\eta)\right)d\eta}{\int\limits_0^1 \left(2\eta - \eta^2\right)\left(\Pr Le\,\dfrac{G_n^{\;2}(1)}{F_n^{\;2}(1)}F_n^{\;2}(\eta) + Sc\Lambda G_n^{\;2}(\eta)\right)d\eta} \tag{49}$$

561

562 As a result, temperature and mass fraction fields are expressed
563 in eq.s 50 and 51.

564

$$565 \quad T(\varepsilon,\eta) = T_W + \left(T_e - T_W\right)\sum_{n=1}^{\infty}\left[A_n\sum_{i=0}^{\infty}\left(a_{n,i}\eta^i\right)e^{-\lambda_n^{\;2}d^*\left(\frac{4WR}{3\mathrm{Re}}\right)^{4/3}\int_0^\varepsilon \sin^{1/3}\pi\varepsilon\,d\varepsilon}\right] \tag{50}$$

$$566 \quad \omega(\varepsilon,\eta) = \omega_e + \left(\omega_{in} - \omega_e\right)\sum_{n=1}^{\infty}\left[B_n\sum_{i=0}^{\infty}\left(b_{n,i}\eta^i\right)e^{-\lambda_n^{\;2}d^*\left(\frac{4WR}{3\mathrm{Re}}\right)^{4/3}\int_0^\varepsilon \sin^{1/3}\pi\varepsilon\,d\varepsilon}\right] \tag{51}$$

567

568 **4. Results**

569 The following analysis is performed for a set of representative
570 operative conditions of the absorber in a cooling system (Table
571 1) and LiBr–H$_2$O solution properties (49) are calculated for the
572 values of temperature, pressure, and mass fraction. Subsequently,
573 the main influential dimensionless parameters are calculated and
574 listed in Table 2.

575

576 **Table 1. Operative conditions**

T_{in} (ºC)	T_W (ºC)	ω_{in} (%)	P (kPa)	r (m)	β Ref. (39)
40	32	60	1.0	0.0090	32 º

577

578 **Table 2. Operative dimensionless parameters**

| Le	Λ	Sc	Pr	d*	Re	Re$_0$
110.8	5.515	2567	23.17	568.4	42.95	95.00

579

580 Figures 3(a) and 3(b) compare temperature and mass fraction
581 fields, respectively, as obtained with the first 9
582 eigenvalues/eigenfunctions of the present analytical solution
583 (Table 3) to the corresponding numerical solutions of energy and
584 species transport equations. Both fields indicate good agreement.
585 However, the temperature distribution specifically appears as a
586 rough approximation at the entrance region in proximity to the
587 wall ($\varepsilon \sim 0$), where the highest deviations with respect to the
588 numerical results are observed.
589
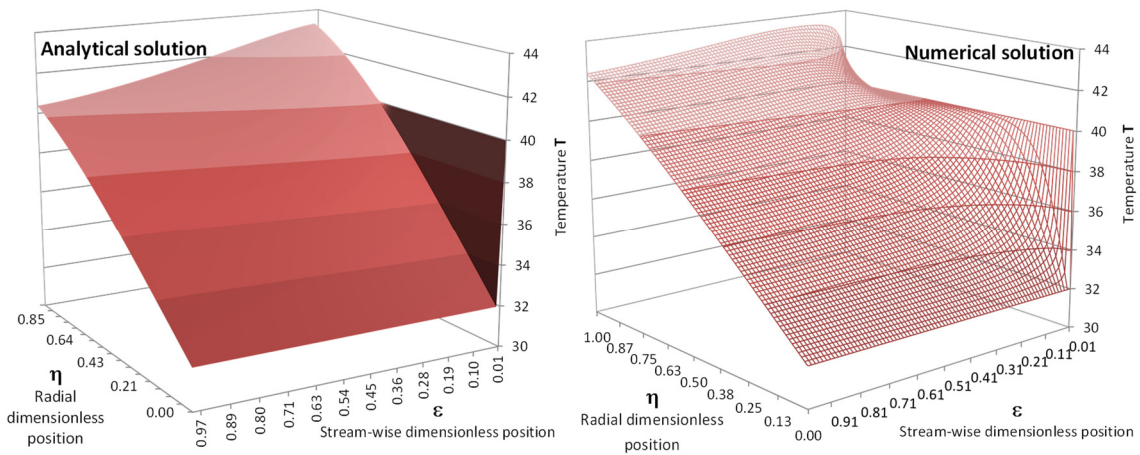
590
591 (a)
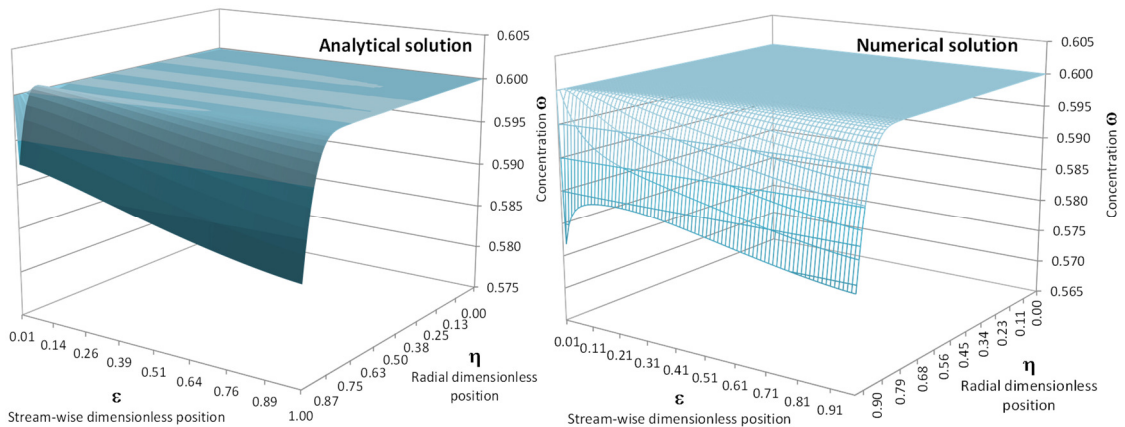
592
593 (b)
594 **Figure 3. Film temperature (a) and mass fraction (b) fields in the operative conditions listed in**
595 **Table 1**
596
597 It is noteworthy to highlight the agreement between the two
598 solution methods at the film interface, where two different

599 equilibrium relations are employed. Equation 23 is used for
600 writing the analytical solution, whereas, the thermo–physical
601 properties from (49) are used when numerically solving eq.s 10
602 and 11. A larger number of eigenvalues and terms representing the
603 eigenfunctions F_n and G_n are considered, and it is possible to
604 model the entrance region with increased accuracy. However, in
605 the case of a subcooled or superheated inlet solution, given the
606 very small values of the coefficient B_n for eigenvalues higher
607 than 9 (Table 3), which goes beyond the number of significant
608 figures available on the calculation platform, this creates
609 instability of the analytical solution away from the wall and
610 specifically close to the film interface (η=1).
611 The temperature field close to the tube surface obtained with the
612 first 14 eigenvalues (Table 4) is compared to the corresponding
613 numerical solution in Figure 4. It is observed that this enables
614 the analytical solution to model the gradual transition of the
615 temperature distribution at the entrance region in proximity to
616 the wall. Hence, the heat transfer at the tube surface is
617 estimated by considering 14 eigenvalues as listed in Table 3.

618
619

Table 3. Eigenvalues and eigenfunction coefficients

n	λ_n	A_n	B_n
1	0.0418	0.129	1.34
2	0.116	0.133	-0.551
3	0.189	0.154	0.369
4	0.259	0.176	-0.275
5	0.326	0.168	0.196
6	0.392	0.113	-0.121
7	0.462	0.0536	0.0610
8	0.533	0.0194	-0.0243
9	0.607	0.00328	0.00440
10	2.26	1.28	-9.00E-45
11	3.06	-0.368	-1.00E-70
12	3.91	1.26	-3.00E-45
13	4.72	-0.504	-1.00E-107
14	5.53	1.27	-8.00E-121

620

Analytical solution — Temperature T, Stream-wise dimensionless position ε, Radial dimensionless position η

Numerical solution — Temperature T, Stream-wise dimensionless position ε, Radial dimensionless position η

621

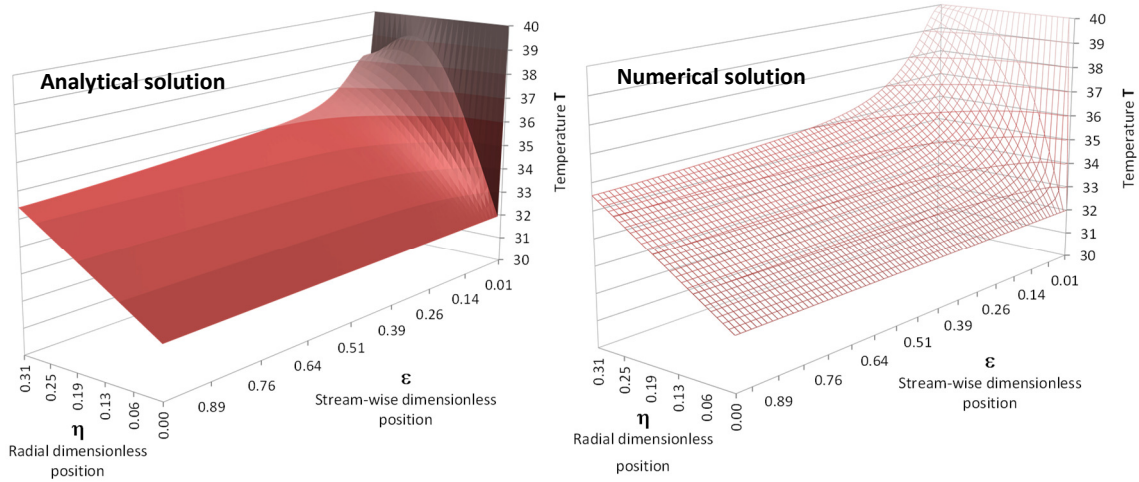**Figure 4. Film temperature field in proximity to the tube wall**

623

5. Heat and mass transfer coefficients

It is assumed that the reduction of the surface in the vapour absorption is represented by the values of WR, and thus the local heat and mass transfer coefficient (htc and mtc) are defined by eq. 52 and eq. 53, respectively, and by eq. 54 and eq. 55, respectively, with respect to the dimensionless parameters (i.e., Nusselt and Sherwood Numbers).

631

$$htc = WR \frac{k \left.\frac{\partial T}{\partial y}\right|_W}{T_{av} - T_W} \tag{52}$$

$$mtc = -WR \frac{D}{\omega_{if}} \frac{\left.\frac{\partial \omega}{\partial y}\right|_{if}}{\omega_W - \omega_{if}} \tag{53}$$

$$Nu(\varepsilon) = \left(\frac{4}{3} \frac{WR^4 \sin \pi \varepsilon}{\mathrm{Re}}\right)^{1/3} \frac{\displaystyle\sum_{n=1}^{\infty} \left[\frac{G_n(1)}{F_n(1)} B_n a_{n,1} e^{-\lambda_n^2 d^* \left(\frac{4WR}{3\mathrm{Re}}\right)^{4/3} \int_0^\varepsilon \sin^{1/3} \pi \varepsilon \, d\varepsilon}\right]}{\displaystyle\sum_{n=1}^{\infty} \left[\frac{G_n(1)}{F_n(1)} B_n \sum_{i=0}^{\infty} \left(\frac{a_{n,i}}{i+1}\right) e^{-\lambda_n^2 d^* \left(\frac{4WR}{3\mathrm{Re}}\right)^{4/3} \int_0^\varepsilon \sin^{1/3} \pi \varepsilon \, d\varepsilon}\right]} \tag{54}$$

$$Sh(\varepsilon) =$$

635

$$\frac{\left(\dfrac{4}{3}\dfrac{WR^4\sin\pi\varepsilon}{\mathrm{Re}}\right)^{1/3}}{\left\{\omega_e+(\omega_{in}-\omega_e)\sum\limits_{n=1}^{\infty}\left[B_n\sum\limits_{i=0}^{\infty}(b_{n,i})e^{-\lambda_n^{2}d^*\left(\frac{4WR}{3\mathrm{Re}}\right)^{4/3}\int_0^{\varepsilon}\sin^{1/3}\pi\varepsilon\,d\varepsilon}\right]\right\}}\cdot\frac{\sum\limits_{n=1}^{\infty}\left[B_n\sum\limits_{i=1}^{\infty}(ib_{n,i})e^{-\lambda_n^{2}d^*\left(\frac{4WR}{3\mathrm{Re}}\right)^{4/3}\int_0^{\varepsilon}\sin^{1/3}\pi\varepsilon\,d\varepsilon}\right]}{\sum\limits_{n=1}^{\infty}\left[B_n\sum\limits_{i=1}^{\infty}(b_{n,i})e^{-\lambda_n^{2}d^*\left(\frac{4WR}{3\mathrm{Re}}\right)^{4/3}\int_0^{\varepsilon}\sin^{1/3}\pi\varepsilon\,d\varepsilon}\right]}$$

636 $\hspace{10cm}$ (55)

637

638 The denominators of these last two expressions represent the

639 driving potentials for heat transfer and that for mass transfer,

640 respectively; in the analytical formulation of the Nusselt

641 number, corresponding to the temperature difference between the

642 bulk value of the liquid film and the solid wall; in the

643 expression of the Sherwood number, the difference between the

644 mass fraction at the interface and at the tube wall. On the

645 right-side of the expressions, the numerators include terms

646 corresponding to the temperature gradient at the tube wall and

647 the mass fraction gradient at the film interface. Hence, the

648 factors on the extreme left-side embody the products of the

649 active extension of the film interface and the inverse of the

650 variation of the film thickness while normalised with respect to

651 the characteristic length L_C.

652 First, the inferences of the main parameters are locally

653 examined for the reference conditions of the absorber as listed

654 in Table 1, and the results obtained are compared while

655 considering the effect of partial wetting (continuous lines)

656 with the solution obtained when the effect is ignored (dashed

657 lines). Figure 5 describes the local Nusselt number distribution

658 along the tube surface. The large temperature difference between

659 the tube wall and the impinging solution at the entrance region

660 is responsible for a local peak in the Nusselt number.

661 Additionally, a local maximum that is positioned in proximity of

662 the vertical part of the tube ($\varepsilon\sim0.5$) is ascribed to the minimum

663 film thickness. Conversely, in the second half of the tube, the

664 thickening of the film is associated to a decreasing trend of
665 the local Nusselt number. It is also stated that higher
666 flowrates extend the region affected by the development of the
667 thermal boundary-layer and are responsible for moving the first
668 local minimum of the heat transfer coefficient to higher stream-
669 wise positions. This trend matches the trend presented in extant
670 studies when the governing equations of horizontal tube falling
671 film absorption are numerically solved (16), and the highest
672 deviation occurs in proximity of the inlet of the calculation
673 domain in which the temperature gradient is steeper due to the
674 boundary condition of constant tube wall temperature. The
675 discrepancy between the analytical solution and the numerical
676 solution of the governing equations (eqs. 10-11) increases when
677 the solution flowrate increases. The remaining deviations are
678 related to the assumption of a linear equilibrium-relationship
679 at the interface.

680

681
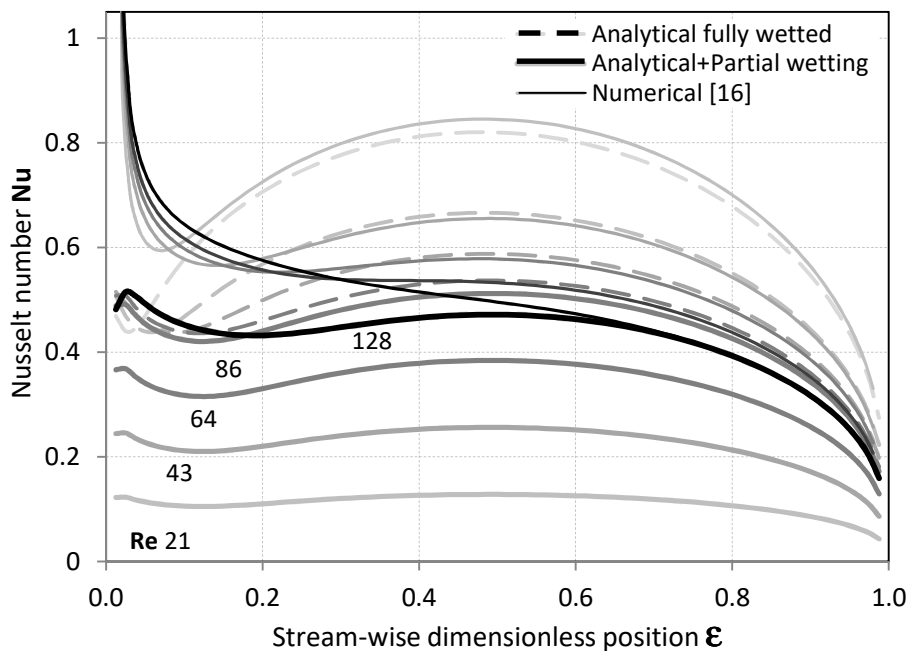
**Figure 5. Local Nusselt number corresponding to the first 14 eigenfuntions for different solution
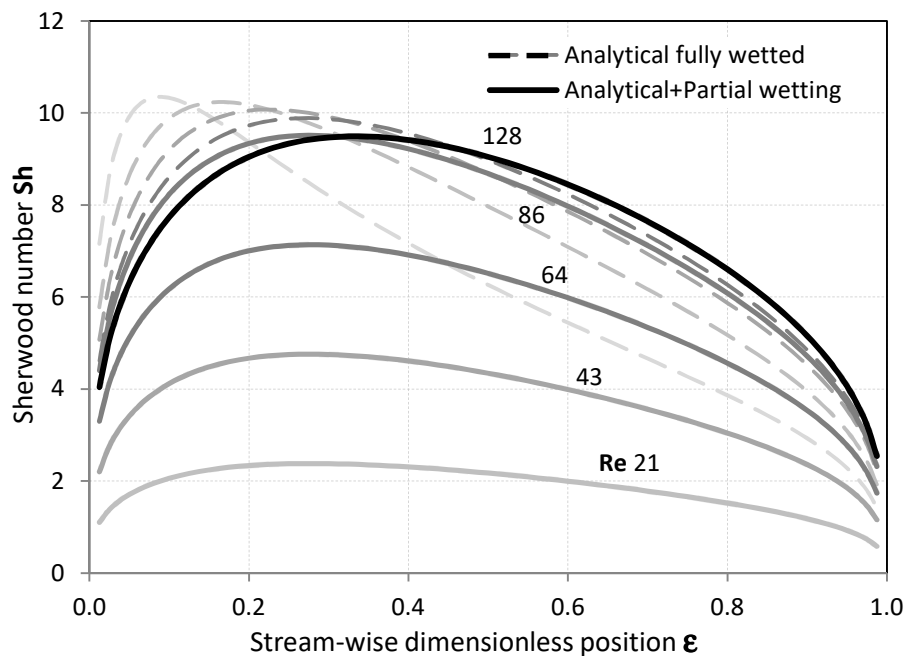mass flowrates at the reference conditions of a refrigerating machine**

684

685 Figure 5 shows a comparison of continuous and dashed lines of
686 corresponding colours and highlights that low Reynolds

687 conditions are associated with a globally higher heat transfer
688 rate if partial wetting is overlooked while a gradual reduction
689 in the heat transfer coefficient that is mainly related to the
690 decreasing wetting ability of the solution is experimentally
691 observed (7–11).

692 In figure 6, the mass transfer at the film interface is locally
693 considered in terms of Sherwood number and indicates a maximum
694 value that grows and moves forward when the solution flowrate
695 increases in the partial wetting region (as shown by the
696 continuous lines).

697

698
699 **Figure 6. Local Sherwood number for different solution mass flowrates at the reference conditions**
700 **of a refrigerating machine**

701

702 Table 4 displays the eigenvalues and their respective
703 eigenfunctions coefficients for two different temperatures at
704 the tube wall of the absorber. A change in this parameter causes
705 the eigenvalues from the characteristic equation (eq. 32) and
706 eigenfunctions coefficients to assume different values.

707

708 **Table 4. Eigenvalues and coefficients with wall temperatures corresponding to 28℃ and 36℃**

n		λ_n	A_n	B_n		λ_n	A_n	B_n
1		0.0424	0.103	1.35		0.0409	0.171	1.33
2		0.118	0.112	-0.571		0.114	0.162	-0.517
3		0.191	0.144	0.407		0.186	0.156	0.310
4		0.262	0.199	-0.337		0.256	0.137	-0.196
5		0.327	0.231	0.271		0.325	0.0971	0.113
6		0.391	0.168	-0.185		0.395	0.0477	-0.0497
7	T_W 28℃	0.459	0.0819	0.105	T_W 36℃	0.465	0.00537	0.00543
8		0.531	0.0368	-0.0554		0.537	-0.0205	0.0207
9		0.605	0.0177	0.0296		0.609	-0.0340	-0.0345
10		2.23	1.40	-1.E-43		2.30	0.991	-3.E-46
11		3.03	-0.282	-9.E-70		3.10	-0.419	-1.E-71
12		3.83	1.24	-4.E-89		3.90	1.06	-8.E-91
13		4.63	-0.316	-4.E-106		4.70	-0.597	-4.E-107
14		5.45	1.20	-2.E-119		5.51332	1.18	-2.E-120

709

710 As a rule, a lower wall temperature enhances heat and mass
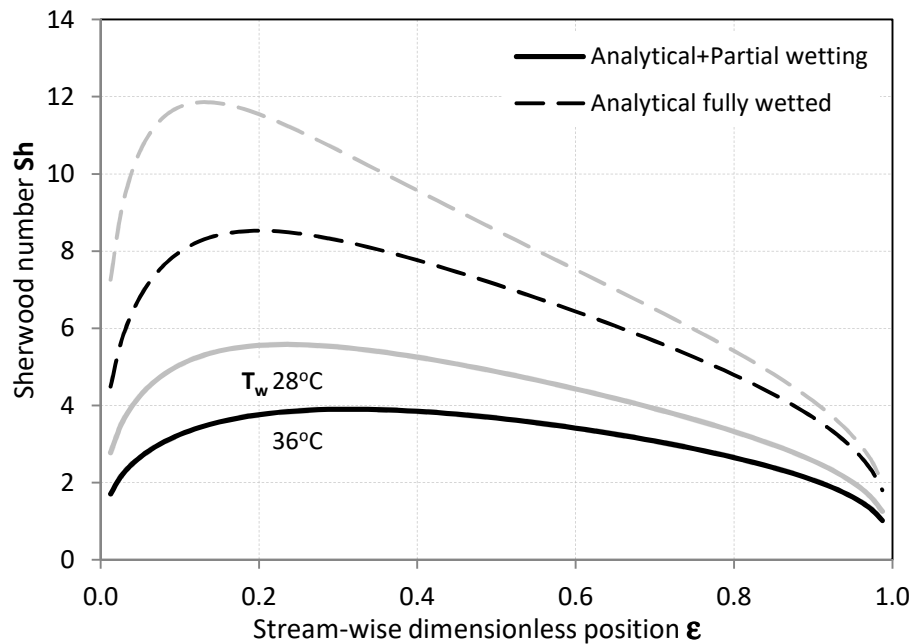711 transfer both locally (Figures 7-8) and globally.

712
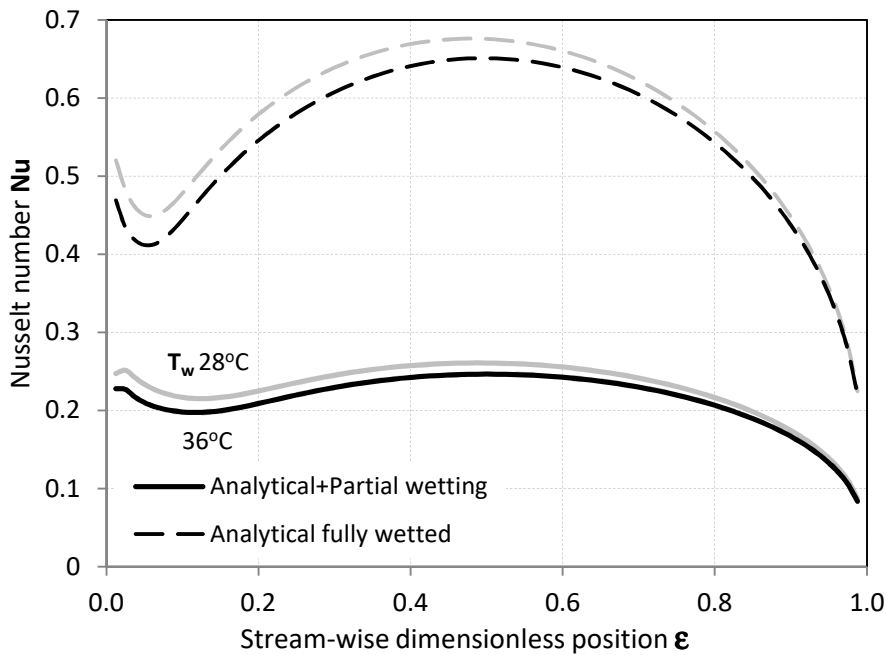
713

714 **Figure 7. Local Nusselt number for different T_W at reference conditions of a refrigerating machine**

715

Figure 8. Local Sherwood number for different tube T_W at reference conditions of a refrigerating machine

The wall temperature affects the Sherwood number through the interfacial temperature and consequently changes the interface mass fraction due to the equilibrium hypothesis. Therefore, a lower heat sink temperature can significantly enhance the system capacity by increasing the amount of refrigerant that steadily circulates within the system for a specific solution flowrate. A local analysis further suggests (50) that a lower tube radius globally increases heat and mass transfer coefficients although it reduces the heat flux per unit length due to a lower heat transfer surface. Accordingly, the best selection of the tube size results from a compromise between the conflicting effects. The local values of *htc* and *mtc* around the tube are averaged to perform a global analysis for the absorber tube in a wide range of flowrates. Figures 9 and 10 show that heat and mass transfer coefficients are maximised at a certain solution mass flowrate based on the extension of the region affected by partial wetting.
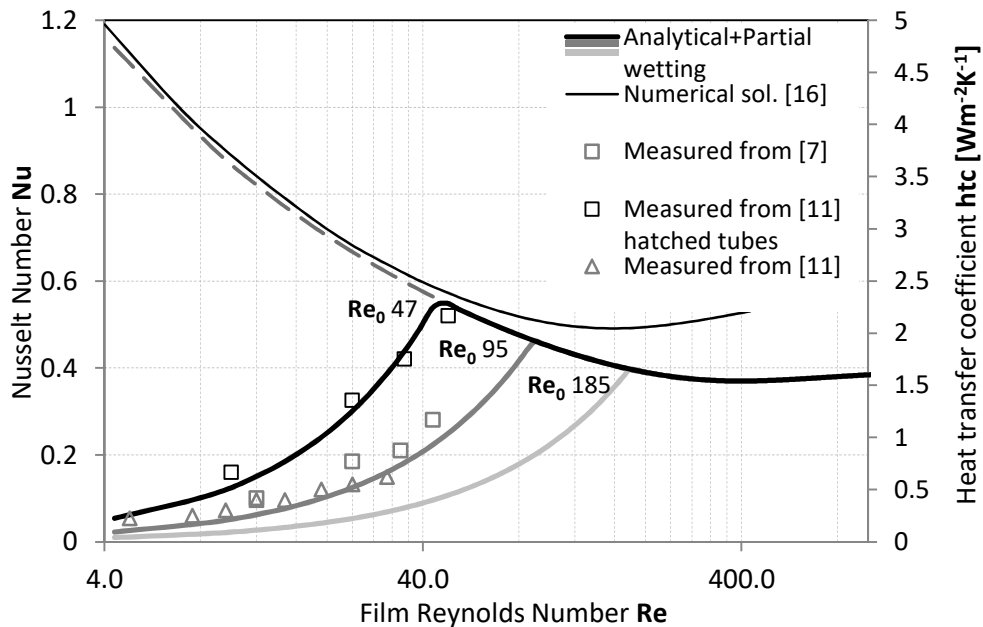
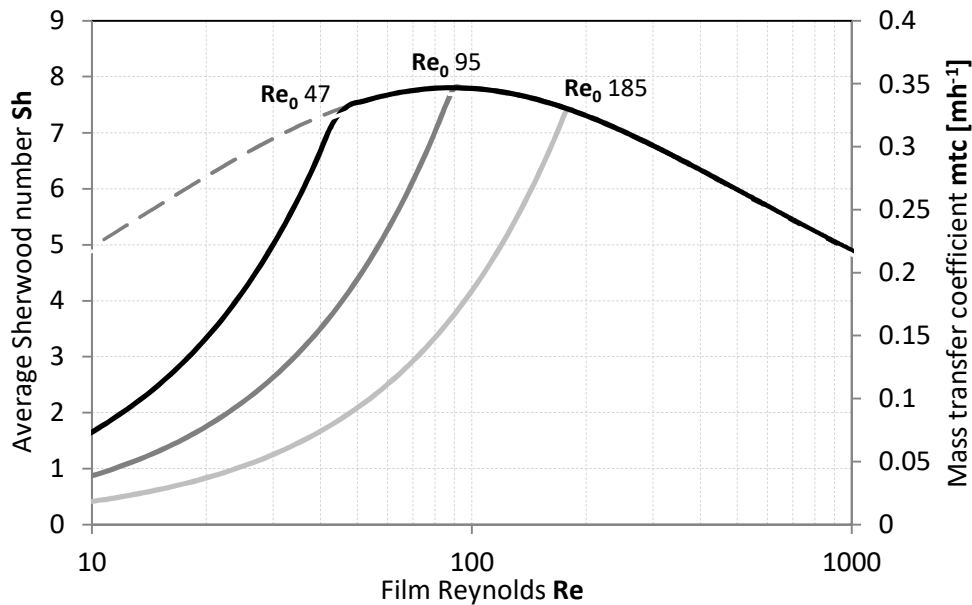**Figure 9. Global Nusselt Number for different wetting behaviours at the reference conditions of a refrigerating machine**

The wettability of LiBr–H_2O solution (eq. 5) is increased if tensioactive substances are added to the mixture to decrease the surface tension σ at the vapour–liquid interface or if the solid surface is properly treated (11) to lower the contact angle β at the solid liquid interface. This stabilises thinner uniform films (eq. 4) and moves the occurrence of the film breaking at a lower Reynolds number Re_0. In contrast, if the affinity between the tube surface and the solution worsens, dry patches also appear at higher Reynolds numbers due to impurities or surface roughness. These two cases are qualitatively represented by the lines labelled as Re_0 47 (the simulations are performed by considering $\beta'=\beta/2$) and Re_0 185 ($\beta''=2\beta$) in figures 9 and 10, respectively, while Re_0 95 represents the case of smooth tubes at reference conditions for a Lithium–Bromide refrigeration machine (Table 1). The dashed line and thin continuous line represent the analytical solution and the numerical results obtained, respectively, when partial wetting ($WR=1$) over the entire range of operative conditions is neglected.

759 Generally, it is highlighted that both heat and mass transfer
760 are critically improved by improving solution wettability. In
761 the case in which a partial wetting model is not included, the
762 simulated heat transfer coefficients follow an increasing trend
763 to decrease the solution mass flowrates. However, this behaviour
764 is in disagreement with all the experimental results indicated in
765 previous studies (5–11). This indicates the necessity to consider
766 partial wetting phenomena in the standard operative range of
767 absorbers operating in real plants.

768

770 **Figure 10. Global Sherwood number for different wetting behaviours at reference conditions of a**
771 **refrigerating machine**

772

773 **7. Conclusions**

774 The presented model for laminar falling film absorption over a
775 horizontal cooled tube considers the cylindrical shape of the
776 tube, the effect of partial wetting, thickness variation of the
777 film flowing around the tube, and arbitrarily selected inlet
778 conditions. A simplified linear model for partial wetting is
779 included to extend the validity of the obtained expressions when
780 complete wetting is not considered as a valid assumption. The
781 model provides detailed information to locally and globally

782 characterise heat and mass transfer of falling film absorbers.
783 The effects related to partial wetting and the main geometrical
784 and operative parameters are investigated to extract general
785 guidelines to optimise the aforementioned devices.
786 Low Reynolds conditions are associated with a globally higher
787 heat transfer rate when partial wetting is overlooked.
788 Conversely, a gradual reduction in the heat transfer coefficient
789 that was mainly related to the decreasing wetting ability of the
790 solution was experimentally observed in previous studies. In
791 general, the results highlight that both heat and mass transfer
792 are critically improved by improving solution wettability.
793 The study indicates the possibility of an optimal tube radius
794 from a compromise between lower heat flux per unit length and
795 higher heat and mass transfer coefficients.
796 Average heat and mass transfer coefficients around the tube are
797 analysed in a wide range of flowrates and show that heat and
798 mass transfer coefficients are maximised at a certain solution
799 mass flowrate based on the extension of the region affected by
800 partial wetting.
801 Given the observed qualitative and quantitative agreements, it is
802 possible to employ the model as a computationally light and
803 accurate module in component and system simulations to design and
804 control actual systems.
805

806 **References**

807 (1)   A. Lubis, J. Jeong, K. Saito, N. Giannetti, H. Yabase, M.I. Alhamid, Nasruddin, (2016),
808 Solar-assisted single-double-effect absorption chiller for use in Asian tropical climates,
809 Renewable Energy, Vol. 99, pp. 825–835.
810 (2)   N. Giannetti, A. Rocchetti, K. Saito, (2016), Thermodynamic optimization of three-
811 thermal irreversible systems, International Journal of Heat and Technology, Vol. 34, pp. S83–
812 S90.
813 (3)   N. Giannetti, A. Rocchetti, A. Lubis, K. Saito, S. Yamaguchi, (2016), Entropy
814 parameters for falling film absorber optimization, Applied Thermal Engineering, Vol. 93, pp.
815 750–762.

816 (4)   N. Giannetti, A. Rocchetti, K. Saito, S. Yamaguchi, (2015), Irreversibility analysis of
817 falling film absorption over a cooled horizontal tube, International Journal of Heat and Mass
818 Transfer, Vol. 88, pp. 755–765.

819 (5)   K. Saito, N. Inoue, Y. Nakagawa, Y. Fukusumi, H. Yamada, T. Irie, (2015),
820 Experimental and numerical performance evaluation of double-lift absorption heat transformer,
821 Science and Technology for the Built Environment, Vol. 21, pp. 312–322.

822 (6)   A. Lubis, N. Giannetti, S. Yamaguchi, K. Saito, N. Inoue, (2017), Experimental
823 performance of a double-lift absorption heat transformer for manufacturing-process steam
824 generation, Energy Conversion and Management, Vol. 148, pp. 267-278.

825 (7)   L. Hoffmann, I. Greiter, A. Wagner, V. Weiss, G. Alefeld, (1996), Experimental
826 investigation of heat transfer in a horizontal tube falling film absorber with aqueous solutions of
827 LiBr with and without surfactants, International Journal of Refrigeration, Vol. 19 (5), pp. 331–
828 341.

829 (8)   I. Kyung, K.E. Herold, Y.T. Kang, (2007), Experimental verification of H_2O/LiBr
830 absorber bundle performance with smooth horizontal tubes, International Journal of
831 Refrigeration, Vol. 30 (4), pp. 582–590.

832 (9)   V.M. Soto Francés, J.M. Pinazo Ojer, (2003), Validation of a model for the absorption
833 process of H_2O(vap) by a LiBr(aq) in a horizontal tube bundle using a multi-factorial analysis,
834 International Journal of Heat and Mass Transfer, Vol. 46, pp. 3299–3312.

835 (10)   S.M. Deng, W.B. Ma, (1999), Experimental studies on the characteristics of an absorber
836 using LiBr/H_2O solution as working fluid, International Journal of Refrigeration, Vol. 22, pp.
837 293–301.

838 (11)   C.W. Park, S.S. Kim, H.C. Cho, Y.T. Kang, (2003), Experimental correlation of falling
839 film absorption heat transfer on micro-scale hatched tubes, International Journal of
840 Refrigeration, Vol. 26 (7), pp.758–763.

841 (12)   S.S. Kim, C.W. Park, H.C. Cho, Y.T. Kang, (2003), The effect of micro-scale surface
842 treatment on heat and mass transfer performance for a falling film H2O/LiBr absorber,
843 International Journal of Refrigeration, Vol. 26 (5), pp. 575–585.

844 (13)   M. Mittermaier, P. Schulze, F. Ziegler, (2014), A numerical model for combined heat
845 and mass transfer in a laminar liquid falling film with simplified hydrodynamics, International
846 Journal of Heat and Mass Transfer, Vol. 70, pp. 990–1002.

847 (14)   J.W. Andberg, G.C. Vliet, (1987), A simplified model for absorption of vapors into
848 liquid films flowing over cooled horizontal tubes, ASHRAE Trans, Vol. 93, pp. 2454–66.

849   (15)   V.D. Papaefthimiou, I.P. Koronaki, D.C. Karampinos, E.D. Rogdakis, (2012), A novel

850   approach for modelling LiBr–H_2O falling film absorption on cooled horizontal bundle of tubes,

851   International Journal of Refrigeration, Vol. 35 (4), pp. 1115–1122.

852   (16)   F. Babadi, B. Farhanieh, (2005), Characteristics of heat and mass transfer in vapor

853   absorption of falling film flow on a horizontal tube, International Communications in Heat and

854   Mass Transfer, Vol. 32 (9), pp.1253–1265.

855   (17)   G. Kocamustafaogullari, I.Y. Chen, (1988), Falling film heat transfer analysis on a bank

856   of horizontal tube evaporator, AIChE Journal, Vol. 34 (9), pp. 1539–1549.

857   (18)   L. Harikrishnan, S. Tiwari, M.P. Maiya, (2011), Numerical study of heat and mass

858   transfer characteristics on a falling film horizontal tubular absorber for R-134a-DMAC,

859   International Journal of Thermal Sciences, Vol. 50 (2), pp. 149–159.

860   (19)   V. Subramaniam, S. Garimella, (2014), Numerical study of heat and mass transfer in

861   lithium bromide-water falling films and droplet, International Journal of Refrigeration, Vol. 40,

862   211–226.

863   (20)   V. Subramaniam, S.rinivas Garimella, (2009), From measurements of hydrodynamics

864   to computation of species transport in falling films, International Journal of Refrigeration, Vol.

865   32 (4), pp. 607–626.

866   (21)   Q. Qiu, C. Meng, S. Quan, W. Wang, (2017), 3-D simulation of flow behaviour and

867   film distribution outside a horizontal tube, International Journal of Heat and Mass Transfer, Vol.

868   107, pp. 1028-1034.

869   (22)   S.M. Hosseinnia, M. Naghashzadegan, R. Kouhikamali, (2016), CFD simulation of

870   adiabatic water vapor absorption in large drops of water–LiBr solution, Applied Thermal

871   Engineering, Vol. 102, pp. 17-29.

872   (23)   Y. Zhou, Z. Cai, Z. Ning, M. Bi, (2017), Numerical simulation of double-phase coupled

873   heat transfer process of horizontal-tube falling film evaporation, Applied Thermal Engineering,

874   Vol. 118, pp. 33-40.

875   (24)   S.M. Hosseinnia, M. Naghashzadegan, R. Kouhikamali, (2017), CFD simulation of

876   water vapor absorption in laminar falling film solution of water-LiBr — Drop and jet modes,

877   Applied Thermal Engineering, Vol. 115, pp. 860-873.

878   (25)   G. Ji, J. Wu, Y. Chen, G. Ji, (2017), Asymmetric distribution of falling film solution

879   flowing on hydrophilic horizontal round tube, International Journal of Refrigeration, Vol. 78, pp.

880   83-92.

881 (26)   N.I. Grigor'eva, V.E. Nakoryakov, (1977), Exact solution of a combined Heat- and

882 Mass- transfer problem during film absorption, Inzhernerno-Fizicheskii Zhurnal, Vol. 33 (5), pp.

883 893–898.

884 (27)   S. K. Choudhury, A. Nishiguchi, D. Hisajima, T. Fukushima, T. ohuchi, S. Sakaguchi,

885 (1993), Absorption of vapors into liquid films flowing over cooled horizontal tubes, ASHRAE

886 Transaction, Vol. 99 (2), pp. 81–89.

887 (28)   G. Grossman, (1983), Simultaneous heat and mass transfer in film absorption under

888 laminar flow, International Journal of Heat and Mass Transfer, Vol. 26 (3), pp. 357–371.

889 (29)   T. Meyer, F. Ziegler, (2014), Analytical solution for combined heat and mass transfer in

890 laminar falling film absorption using first type boundary conditions at the interface,

891 International Journal of Heat and Mass Transfer, Vol. 73, pp. 141–151.

892 (30)   M.J. Kirby, H. Perez-Blanco, (1994), A Design Model for Horizontal Tube

893 Water/Lithium Bromide Absorbers, Heat pump and refrigeration systems design, analysis, and

894 applications, ASME-PUBLICATIONS- AES, Vol. 32, pp. 1-10.

895 (31)   J. Wu, Z. Yi, Y. Chen, R. Cao, C. Dong, S. Yuan, (2015), Enhanced heat and mass

896 transfer in alternating structure of tubes and longitudinal trough mesh packing in lithium

897 bromide solution absorber, International Journal of Refrigeration, Vol. 53, pp. 34-41.

898 (32)   S. Jeong, S. Garimella, (2002), Falling-film and droplet mode heat and mass transfer in

899 a horizontal tube LiBr/water absorber, International Journal of Heat and Mass Transfer, Vol. 45

900 (7), pp. 1445–1458.

901   (33)   V. M. Soto Francés, J. M. Pinazo Ojer, Experimental study about heat and mass transfer

902 during absorption of water by an aqueous lithium bromide solution, International Proceedings of

903 the ASME-ZSITS International Thermal Science Seminar, Bled (Slovenia), 11–14 June, (2000),

904 pp. 535–542.

905 (34)   N. Giannetti, A. Rocchetti, S. Yamaguchi, K. Saito, (2017), Analytical solution of film

906 mass-transfer on a partially wetted absorber tube, International Journal of Thermal Sciences,

907 Vol. 118, pp. 176-186.

908 (35)   Y. Chen, R. Cao, J. Wu, Z. Yi, G. Ji, (2016), Alternate heat and mass transfer

909 absorption performances on staggered tube bundle with M–W corrugated mesh guider inserts,

910 International Journal of Refrigeration, Vol. 66, pp. 10-20.

911 (36)   R.H. Wassenaar, (1996), Measured and predicted effect of flowrate and tube spacing on

912 horizontal tube absorber performance, International Journal of Refrigeration, Vol. 19 (5), pp.

913 347–355.

914   (37)   Y. Lazcano-Véliz, J. Siqueiros, D. Juárez-Romero, L.I. Morales, J. Torres-Merino,
915   (2014), Analysis of effective wetting area of a horizontal generator for an absorption heat
916   transformer, Applied Thermal Engineering, Vol. 62 (2), pp. 845–849.

917   (38)   K.S. Lee, B. Köroğlu, C. Park, (2012), Experimental investigation of capillary-assisted
918   solution wetting and heat transfer using a micro-scale, porous-layer coating on horizontal-tube,
919   falling-film heat exchanger, International Journal of Refrigeration, Vol. 35 (4), pp. 1176–1187.

920   (39)   B. Köroğlu, K.S. Lee, C. Park, (2013), Nano/micro-scale surface modifications using
921   copper oxidation for enhancement of surface wetting and falling-film heat transfer, International
922   Journal of Heat and Mass Transfer, Vol. 62, pp. 794–804.

923   (40)   D. M. Maron, G. Ingel, N. Brauner, (1982), Wettability and break-up of thin films on
924   inclined surfaces with continuous and intermittent feed, Desalination, Vol. 42, pp. 87–96.

925   (41)   J. Tang, Z. Lu, B. Yu-Chi, S. Lin, (1991), Minimum Wetting Rate of Film Flow on
926   Solid Surface, Proceedings of the 18th International Congress of Refrigeration, Vol. 2, pp. 519–
927   523, Montreal.

928   (42)   J. Mikielewicz, J. R. Moszynski, (1976), Minimum thickness of a liquid film flowing
929   vertically down a solid surface, lnternational Journal of Heat and Mass Transfer, Vol. 19, pp.
930   771–776.

931   (43)   N. Giannetti, S. Yamaguchi, K. Saito, (2016), Wetting behaviour of a liquid film on an
932   internally-cooled desiccant contactor, International Journal of Heat and Mass Transfer, Vol. 101,
933   pp. 958–969.

934   (44)   C.S. Yih, (1963), Stability of liquid flow down an inclined plane, Phyics of Fluids, Vol.
935   6, pp. 321-334.

936   (45)   D.E. Hartley, W. Murgatroyd, (1964), Criteria for the break-up of thin liquid layers
937   flowing isothermally over solid surfaces, International Journal of Heat and Mass Transfer, Vol.
938   7, pp. 1003-1015.

939   (46)   A.B. Ponter, G.A. Davies, T.K. Ross, P.G. Thornley, (1967), The influence of mass
940   transfer on liquid film breakdown, International Journal of Heat and Mass Transfer, Vol. 10, pp.
941   349-359.

942   (47)   N. Giannetti, D. Kunita, S. Yamaguchi, K. Saito, (2018), Annular flow stability within
943   small-sized channels, International Journal of Heat and Mass Transfer, Vol. 116, pp. 1153-1162.

944   (48)   G. Grossmann, (1982), Simultaneous heat and mass transfer in absorption/desorption of
945   gases in laminar liquid films, Proc. A.I.Ch.E. Winter and Annual Meeting, Orlando, Florida.

946   (49)   (1990), properties of lithium bromide-water solutions at high temperatures and
947   condensations - Part I. Thermal Conductivity, ASHRAE Trans, Vol. 96.

948   (50)   N. Giannetti, A. Rocchetti, K. Saito, S. Yamaguchi, (2016), Analytical description of

949   falling film absorption, Proceedings of the 8th Asian Conference on Refrigeration and Air

950   Conditioning, May 15th –17th, Taipei, Taiwan.

951   https://www.scopus.com/inward/record.uri?eid=2-s2.0-

952   84988972662&partnerID=40&md5=72097627e4b8617ef7168d45b30fd3c1